Dynamic-nuclear-polarization method of investigating correlated ESR and NMR strain-broadening effects in single crystals*

C. M. Brodbeck,† Sook Lee, and H. H. Niebuhr‡
Department of Physics, Saint Louis University, St. Louis, Missouri 63103
(Received 12 November 1973; revised manuscript received 6 March 1974)

Quantitative theoretical and experimental investigations are made of the behavior of strain-broadened NMR line shapes under dynamic nuclear polarization (DNP) produced by microwave saturation at the centers of strain-broadened ESR lines where the ESR and NMR strain broadenings are mutually correlated. Based on a phenomenological model, analytical expressions are obtained for the shapes of the NMR lines under DNP. These expressions are found to be in good agreement with experimental data obtained from several ruby (Al_2O_3:Cr^{3+}) crystals.

I. INTRODUCTION

The inhomogeneous broadening of electron-spin-resonance (ESR) and nuclear-magnetic-resonance (NMR) lines due to strains associated with crystalline imperfections is a widely observed phenomenon in solid states.[1–19] This type of line broadening, commonly referred to as strain broadening, is caused by distortions of the crystalline electric field from site to site in the crystal, leading to variations or deviations in the electron- and nuclear-spin coupling constants about the perfect-crystal values. The coupling constants most sensitive to strains are generally those representing the ESR fine-structure and NMR quadrupole-structure interactions.

In quantitative treatments of strain broadening it is widely assumed that the variations of coupling constants are randomly distributed and can be described by a statistical distribution function (e.g., a Gaussian error function) having a suitable linewidth or standard deviation.[1–11] In this approximation, the total linewidth of an ESR or NMR line is treated as the superposition of two widths; one is that due to the strain broadening, and the other is the intrinsic linewidth such as that arising from the spin-spin (electron-electron, electron-nuclear, or nuclear-nuclear) interactions. Thus when the intrinsic linewidth can be calculated for a given crystal structure, the linewidth representing the strain broadening can be extracted from the total linewidth experimentally measured.

In addition to the above method, attempts have been made to associate the detailed shapes of strain-broadened ESR and NMR lines with the specific types of crystalline imperfections producing the strain broadening.[12–19] For instance, it has been predicted theoretically[13,14] that point defects and dislocations give rise to Lorentzian and Gaussian broadenings, respectively, and a number of investigators have been successful in explaining their experimental data based on this type of prediction.[15–19]

Although there are many examples of ESR and NMR work dealing with strain broadening, few studies have been made on solids containing both a dilute electron-spin system and a concentrated nuclear-spin system in which the strain-broadening effects on both spin species are investigated. In certain cases it has been found by means of electron-nuclear double resonance (ENDOR) that the quadrupole coupling constants of the nuclear spins immediately surrounding paramagnetic impurity ions differ from the whole-sample average quadrupole coupling constant.[20,21] These deviations have been attributed to a systematic distortion at the nearby nuclear-spin sites due to the presence of the impurity ions.[20] The ENDOR techniques have also been employed to investigate the correlated strain broadenings between paramagnetic impurity ions and the nuclear spins belonging to these ions.[22]

It is well known that various kinds of crystalline defects, in particular those intrinsic to the host lattice (e.g., dislocations), produce long-range strain fields which extend over many lattice sites.[1,19,23] These long-range strain fields would affect not only the impurity ions but also the bulk of the nuclear spins which are distant from the impurity ions. As a result, it is reasonable to expect that there will be one or more types of correlations between the strain broadenings of the ESR and NMR lines observed from the whole sample. To our knowledge, however, there have been no instances in which such a correlated ESR and NMR strain-broadening effect from the whole sample has been detected and investigated.

Recently, we have reported[24] that the method of dynamic nuclear polarization (DNP) by the Solid Effect can be employed to investigate the correlated ESR and NMR strain broadenings in single crystals. Based on a qualitative model, it has

been shown that the DNP produced by saturating the center portion of a strain-broadened ESR fine-structure line gives rise to unusual line shapes for the strain-broadened NMR quadrupole-structure lines, which depend on the correlation of ESR and NMR strain effects within the locality of each paramagnetic ion. Experimental data on the ^{27}Al NMR quadrupole structures in a single crystal of ruby ($Al_2O_3:Cr^{3+}$) have been found to be consistent with our qualitative model.

In this paper we present some detailed descriptions of the correlated ESR and NMR strain-broadening effect in DNP. These include a quantitative theoretical treatment of the effect which yields an analytic functional form for the shape of the NMR structures under DNP, and a comparison of the theoretical results with the experimental data obtained from a variety of ruby crystals containing different Cr^{3+}-ion concentrations. It will be seen that the DNP method is capable of not only revealing but also characterizing correlations between the strain broadenings of the paramagnetic impurity ions and of the nuclear spins surrounding these ions in single crystals.

II. THEORY

The system pertinent to the present investigation is a diamagnetic single crystal containing a small amount of paramagnetic impurity ions which exhibit a crystal-field, fine-structure splitting, and a concentrated number of nuclear spins which exhibit a quadrupole splitting. It is also essential that the crystal display strain-broadened ESR and NMR lines in the conventional ESR and NMR experiments, as well as produce a sizable DNP by the Solid Effect.

A. ESR and NMR strain broadening

For simplicity, we consider that the paramagnetic ions in the crystal are characterized by the following axially symmetric spin Hamiltonian[25]:

$$\mathcal{H}_e = g_{\parallel}\beta_e H_z S_z + g_{\perp}\beta_e (H_x S_x + H_y S_y) + \mathfrak{D}[S_z^2 - \tfrac{1}{3}S(S+1)] , \quad (1)$$

where $g_{\parallel}$ and $g_{\perp}$ are the components of the spectroscopic splitting g tensor parallel and perpendicular to the symmetry axis (which is taken to be the z axis), and $\mathfrak{D}$ is the fine-structure splitting constant. For the external magnetic field $\vec{H}$ applied parallel to the symmetry axis, the above spin Hamiltonian is diagonal, and the magnetic field values for the $M \leftrightarrow M-1$ ESR transitions are given by[25]

$$H(M \leftrightarrow M-1) = h\nu_e/g_{\parallel}\beta_e \mp |\mathfrak{D}|(2M-1)/g_{\parallel}\beta_e , \quad (2)$$

where M is the magnetic quantum number of the electron spin S, and ν_e is the microwave frequency. In this equation, we use $\mp|\mathfrak{D}|$ to distinguish explicitly the two possible signs of $\mathfrak{D}$, the minus sign applying for a positive, and the plus sign for a negative fine-structure splitting constant $\mathfrak{D}$.

Similarly, we consider that the nuclear-spin system undergoes an axially symmetric quadrupole splitting represented by the following nuclear spin Hamiltonian[26]:

$$\mathcal{H}_n = -g_n\beta_n H_z I_z + \mathfrak{Q}[I_z^2 - \tfrac{1}{3}I(I+1)] , \quad (3)$$

where the z axis (the symmetry axis) is assumed to coincide with the ESR symmetry axis of Eq. (1). In this expression $\mathfrak{Q}$ denotes the quantity $3e^2q\mathfrak{Q}/4I(2I-1)$, where $e^2q\mathfrak{Q}/h$ is ordinarily referred to as the quadrupole coupling constant. For convenience, however, we will call $\mathfrak{Q}$ in Eq. (3) the quadrupole coupling constant throughout this paper. For $\vec{H}$ parallel to the quadrupole symmetry axis, the $m \leftrightarrow m-1$ NMR transition frequencies are given by[26]

$$\nu(m \leftrightarrow m-1) = \nu_n^0 \mp |\mathfrak{Q}|(2m-1) , \quad (4)$$

where m is the magnetic quantum number of the nuclear spin I, and $\nu_n^0 = g_n\beta_n H/h$ is the Larmor or unperturbed NMR frequency. In this equation, we again use the minus sign for a positive, and the plus sign for a negative quadrupole coupling constant $\mathfrak{Q}$.

It should be noted that the values of $\mathfrak{D}$ and $\mathfrak{Q}$ in Eqs. (1) and (3), which are normally determined by ESR and NMR experiments, respectively, represent the whole-sample average values, and hence can be regarded as the coupling constants at the perfect-crystal sites. At crystal sites influenced by strains, the associated crystalline fields vary slightly from those at the perfect-crystal sites. These variations are usually taken into account by incorporating into the spin Hamiltonians of Eqs. (1) and (3), respectively, terms which are quadratic in spin operators,[4,8,27–29]

$$\mathcal{H}_e' = \sum_{i,j}^{3} F_{ij}^e S_i S_j , \quad (5a)$$

$$\mathcal{H}_n' = \sum_{i,j}^{3} F_{ij}^n I_i I_j . \quad (5b)$$

The coefficients F_{ij}^e and F_{ij}^n are the components of symmetric and traceless tensors and depend linearly on the components of lattice strain via the electron and nuclear magnetoelastic strain tensors, respectively. The sums over i and j are taken with respect to the Cartesian components $x=1$, $y=2$, and $z=3$.

When the external magnetic field $\vec{H}$ is imposed parallel to the ESR fine-structure and NMR quadrupole symmetry axes (in the z direction), the only terms of Eqs. (5) which contribute in first order to the shifts in the energy levels are the diagonal

terms. Hence, at this orientation, the traceless property of the tensors F^e_{ij} and F^n_{ij} can be employed to represent the net shifts in the energy levels as

$$\mathcal{H}'_e = \tfrac{3}{2} F^e_{zz}[S_z^2 - \tfrac{1}{3} S(S+1)] , \tag{6a}$$

$$\mathcal{H}'_n = \tfrac{3}{2} F^n_{zz}[I_z^2 - \tfrac{1}{3} I(I+1)] . \tag{6b}$$

These terms are formally identical with the axially symmetric crystal-field interaction of the ions in Eq. (1) and the axially symmetric quadrupole interaction of the nuclear spins in Eq. (3). Thus the spin Hamiltonians which include the strain terms of Eqs. (6a) and (6b) for $\vec{H} \parallel \vec{z}$ can be written as

$$\mathcal{H}''_e = g_{\parallel}\beta_e H_z S_z + \mathfrak{D}'[S_z^2 - \tfrac{1}{3} S(S+1)] , \tag{7a}$$

$$\mathcal{H}''_n = -g_n\beta_n H_z I_z + \mathfrak{Q}'[I_z^2 - \tfrac{1}{3} I(I+1)] , \tag{7b}$$

where

$$\mathfrak{D}' = \mathfrak{D} + \tfrac{3}{2} F^e_{zz} , \tag{8a}$$

$$\mathfrak{Q}' = \mathfrak{Q} + \tfrac{3}{2} F^n_{zz} . \tag{8b}$$

It is apparent from the above Eqs. (7) and (8), that for $\vec{H} \parallel \vec{z}$ the net effect of strains can be characterized in first order entirely by means of deviations in the ESR fine-structure and NMR quadrupole coupling constants from their respective perfect-crystal values. For convenience, we denote these deviations by

$$D = |\mathfrak{D}'| - |\mathfrak{D}| , \tag{9a}$$

$$Q = |\mathfrak{Q}'| - |\mathfrak{Q}| . \tag{9b}$$

Then for a given paramagnetic ion with the deviation D, the resonant magnetic field for the $M \leftrightarrow M-1$ ESR transition of this ion is shifted with respect to the corresponding perfect-crystal value of Eq. (2) by

$$H'(M \leftrightarrow M-1) = aD , \tag{10}$$

where

$$a \equiv \mp (2M-1)/g_{\parallel}\beta_e . \tag{11}$$

Similarly, for a given nuclear spin with the deviation Q, the resonance frequency for the $m \leftrightarrow m-1$ NMR transition of this spin is shifted with respect to the corresponding perfect-crystal value of Eq. (4) by

$$\nu'(m \leftrightarrow m-1) = bQ , \tag{12}$$

where

$$b \equiv \mp (2m-1) . \tag{13}$$

The over-all broadening in the ESR and NMR lines due to strains in the whole sample can be calculated from Eqs. (10) and (12) by assuming specific distributions for the deviations D and Q in the whole sample.

B. Model for the correlated ESR and NMR strain-broadening effect in DNP and a correlation parameter p

As already mentioned, the study of the correlated ESR and NMR strain-broadening effect by the DNP method consists in investigating the behavior of strained-broadened NMR quadrupole structures under the DNP produced by saturating the center portion of a strain-broadened ESR fine-structure line.[24] Under this DNP, the NMR quadrupole structures will exhibit line shapes distinctly different from the thermal-equilibrium NMR line shapes if the strain fields in the vicinity of each ion produce a correlation between the deviation D of the ion and the deviations Q of the nuclear spins surrounding this ion. To treat this phenomenon quantitatively we adopt the following model:

(i) We view the crystal as divided into numerous spheres each of which contains one paramagnetic ion at its center and whose diameter is characterized by the average distance between the paramagnetic ions. Thus the nuclear spins contained within a given sphere are assumed to be influenced only by the paramagnetic ion at the center of this sphere during DNP processes. Within each sphere, we further subdivide the nuclear spins into two groups. One group consists of those nuclear spins distant from the ion which contribute to the experimentally observed NMR signal from the whole sample at thermal equilibrium as well as under DNP. The second group contains those nuclear spins nearby the ion which experience large local fields from the ion so that their Larmor frequencies fall outside the experimentally observed NMR signal from the whole sample. Those nuclear spins in the first group will be considered as being contained within a shell, and this shell will be referred to as a "shell of influence"[30] of the ion in this paper.

(ii) The ESR line arising from each ion is considered to be substantially inhomogeneously broadened by unresolved hyperfine interactions with the nearby nuclear spins. Thus the DNP by the Solid Effect within the shell of influence of each ion is proportional to the negative of the first derivative of this ESR line, based on the standard theory.[31] That is, the NMR signal arising from the nuclear spins within each shell becomes positively enhanced for microwave pumping power applied at magnetic fields higher than the center of the ESR line, whereas it is negatively enhanced at lower fields; at the center of the ESR line the NMR signal is vanishing. For convenience, we define the NMR enhancement at the magnetic field H, $\mathcal{E}(H)$, as the ratio of the NMR intensity under DNP to the thermal-equilibrium NMR intensity at this field H.

(iii) Possible ESR and NMR line broadenings arising from variations in the symmetry axes of

the ESR fine-structure and NMR quadupole interactions associated with mosaic structures in the crystal are taken to be vanishingly small. This situation is realized when the external magnetic field $\vec{H}$ is applied parallel to the symmetry axis in the case of axial symmetry. We also neglect ESR and NMR line broadenings connected with inhomogeneities in the external magnetic field $\vec{H}$.

(iv) The over-all distributions of deviations D and Q in the whole sample due to strains are represented by Gaussian functions of width ΔD and ΔQ centered about $D=0$ and $Q=0$, respectively. That is, the number of paramagnetic ions having deviations between D and $D+dD$ is given by

$$n(D, \Delta D, 0)dD = \frac{1}{(2\pi)^{1/2}\Delta D} \exp\left(\frac{-D^2}{2\,\Delta D^2}\right) dD \ , \quad (14)$$

and the number of nuclear spins having deviations between Q and $Q+dQ$ is given by

$$n(Q, \Delta Q, 0)\,dQ = \frac{1}{(2\pi)^{1/2}\Delta Q} \exp\left(\frac{-Q^2}{2\,\Delta Q^2}\right) dQ \ . \quad (15)$$

The distribution of deviations Q within the shell of influence of a given paramagnetic ion in the crystal is represented by a Gaussian function of width δQ, centered at the average deviation of these nuclear spins, denoted by $\overline{Q}$; that is,

$$n(Q, \delta Q, \overline{Q})\,dQ = \frac{1}{(2\pi)^{1/2}\delta Q} \exp\left(\frac{-(Q-\overline{Q})^2}{2\,\delta Q^2}\right) dQ \ . \quad (16)$$

For simplicity, the width δQ is taken to be the same within all the shells in the crystal, although the average deviation $\overline{Q}$ varies from shell to shell. We also assume that the distribution of $\overline{Q}$ from shell to shell is characterized by a Gaussian function,

$$n(\overline{Q}, \Delta\overline{Q}, 0)\,d\overline{Q} = \frac{1}{(2\pi)^{1/2}\Delta\overline{Q}} \exp\left(\frac{-\overline{Q}^2}{2\,\Delta\overline{Q}^2}\right) d\overline{Q} \ . \quad (17)$$

having a width $\Delta\overline{Q}$. It is seen that the whole-sample width ΔQ of Eq. (15) is considered to arise partly from the width δQ of Eq. (16) for the deviations Q within the shells, and partly from the width $\Delta\overline{Q}$ of Eq. (17) for the average deviations $\overline{Q}$ among the shells. By convoluting Eqs. (16) and (17), the whole-sample width ΔQ can be expressed as the following root-mean-square sum:

$$\Delta Q = (\delta Q^2 + \Delta\overline{Q}^2)^{1/2} \ . \quad (18)$$

(v) The average deviation $\overline{Q}$ in the quadrupole coupling constants of the nuclear spins contained within the shell of influence of a given paramagnetic ion is then correlated with the deviation D in the fine-structure constant of this ion. Since the distribution functions for both $\overline{Q}$ and D are assumed to be Gaussian, this correlation may be characterized by a linear relation of the form

$$\frac{\overline{Q}}{\Delta Q} = p\,\frac{D}{\Delta D} \ , \quad (19)$$

where p is a constant. In this expression, p may be either positive or negative. A positive value of p represents the case that owing to coherent strains in the vicinity of a paramagnetic ion, the ESR fine-structure constant of the ion and the average NMR quadrupole coupling constant of the nuclear spins surrounding this ion are increased simultaneously or decreased simultaneously in magnitude with respect to the perfect-crystal values $|\mathfrak{D}|$ and $|\mathfrak{Q}|$. A negative value of p means that the magnitudes of the ESR and NMR coupling constants are correlated in the reverse direction in that an increase in the magnitude of the ESR fine-structure constant is necessarily coupled with a decrease in the magnitude of the average NMR quadrupole coupling constant, and vice-versa.

Based on the linear correlation of Eq. (19) the distribution function for the deviations D given in Eq. (14) can be written in terms of a distribution function for the average deviations $\overline{Q}$ as

$$n(\overline{Q}, |p|\,\Delta Q, 0)\,d\overline{Q} = \frac{1}{(2\pi)^{1/2}\,|p|\,\Delta Q} \times \exp\left(\frac{-\overline{Q}^2}{2\,p^2\Delta Q^2}\right) d\overline{Q} \ . \quad (20)$$

In order for this expression to be consistent with Eq. (17), the following relation must hold:

$$\Delta\overline{Q} = |p|\,\Delta Q \ . \quad (21)$$

Then combining Eqs. (18) and (21), one obtains

$$\delta Q = (1-p^2)^{1/2}\,\Delta Q \ . \quad (22)$$

This relation restricts p to values ranging from -1 to $+1$.

It is seen from Eqs. (21) and (22) that we have formulated the problem in such a manner that if the whole-sample width ΔQ is known from standard NMR measurements, a determination of the correlation parameters p yields the width $\Delta\overline{Q}$ of the distribution of average deviations $\overline{Q}$ from shell to shell, and the width δQ of the distribution of deviations Q within these shells. Therefore, the parameter p not only characterizes the magnitude and direction of the correlation between the average deviation $\overline{Q}$ and the deviation D of the ion, but also gives the relative contributions to the whole-sample NMR strain broadening arising from coherent, long-range NMR strain effects (characterized by the width $\Delta\overline{Q}$) and from random, short-range NMR strain effects within the shells (characterized by the width δQ).

For example, if $|p|=1$, then from Eqs. (21) and (22), $\Delta Q = \Delta\overline{Q}$ and $\delta Q = 0$. In this case the NMR strain broadening from the whole sample is accounted for entirely by the distribution of average

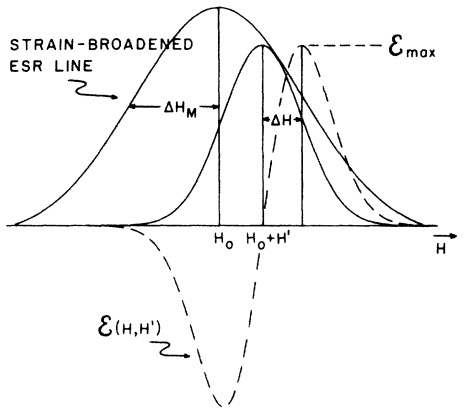

FIG. 1. Strain-broadened ESR fine-structure line, of linewidth ΔH_M, consisting of many ESR component lines each characterized by the intrinsic rigid-lattice linewidth ΔH. The dashed line centered at $H=H_0+H'$ represents the NMR enhancement arising from the Solid Effect associated with the ESR component line at $H=H_0+H'$.

deviations $\bar{Q}$ from shell to shell. Since $\delta Q=0$, all the nuclear spins within the shell of influence of a given ion have the same deviation $\bar{Q}$, which is correlated in turn with the deviation D of this ion. On the other hand if $p=0$, then $\Delta\bar{Q}=0$ and $\Delta Q=\delta Q$. Thus the entire NMR strain broadening arises from the deviations Q within the shells due to short-range uncorrelated strain effects. The case $p=0$ also represents no correlation between $\bar{Q}$ and D within the shells.

C. Shapes of NMR quadrupole lines under DNP and the absolute sign of p

On the basis of the model established in Sec. IIB we now calculate the shapes of the NMR quadrupole component lines from the whole sample under DNP at the center of a strain-broadened ESR fine-structure line. This calculation requires first that the shape functions be fixed for the ESR and NMR lines representing intrinsic line broadenings arising from the rigid-lattice electron-electron, electron-nuclear, and nuclear-nuclear interactions. For simplicity, we assume these shape function to be all Gaussian.

For the nuclear spin with the deviation Q in its quadrupole coupling constant, the Gaussian shape function for the $m \rightarrow m-1$ NMR transition may be written as

$$g(\nu-\nu')=\frac{A_m}{(2\pi)^{1/2}\Delta\nu_m}\exp\left(\frac{-(\nu-\nu')^2}{2\,\Delta\nu_m^2}\right), \tag{23}$$

where ν' is the frequency shift associated with the deviation Q [see Eq. (12)], A_m is the relative NMR intensity or transition probability[26] which is proportional to $[I(I+1)-m(m-1)]$, and $\Delta\nu_m$ is the intrinsic NMR linewidth due to the rigid-lattice nuclear-nuclear and electron-nuclear interactions for the $m \rightarrow m-1$ NMR transition.

For the group of nuclear spins contained within the shell of influence of a paramagnetic ion with the deviation D, the composite NMR line shape will result by convoluting the shape function $g(\nu-\nu')$ of Eq. (23) with the distribution of frequencies ν' within this shell. This frequency distribution is obtained by expressing Eq. (16) in terms of the frequencies ν' of Eq. (12) giving

$$n(\nu',\delta\nu',\bar{\nu}')\,d\nu'=\frac{1}{(2\pi)^{1/2}\delta\nu'}\exp\left(\frac{-(\nu'-\bar{\nu}')^2}{2\,\delta\nu'^2}\right)d\nu', \tag{24}$$

where $\bar{\nu}'=b\bar{Q}$ and $\delta\nu'=|\,b\,|\,\delta Q$. Employing Eqs. (19) and (22), $\bar{\nu}'$ and $\delta\nu'$ can also be expressed as

$$\bar{\nu}'=bp(\Delta Q/\Delta D)\,D\,, \tag{25}$$

$$\delta\nu'=|\,b\,|\,(1-p^2)^{1/2}\,\Delta Q\,. \tag{26}$$

The resultant thermal-equilibrium NMR line-shape function $f(\nu, D)$ for the nuclear spins in the shell of influence of the ion with the deviation D is given by

$$f(\nu,D)=\int_{-\infty}^{\infty}g(\nu-\nu')\,n(\nu',\delta\nu',\bar{\nu}')\,d\nu'\,, \tag{27}$$

which yields

$$f(\nu,D)=\frac{A_m}{\{2\pi[\Delta\nu_m^2+b^2(1-p^2)\,\Delta Q^2]\}^{1/2}}\times\exp\left(\frac{-[\nu-bp\,(\Delta Q/\Delta D)D]^2}{2[\Delta\nu_m^2+b^2(1-p^2)\,\Delta Q^2]}\right). \tag{28}$$

When microwave pumping power is applied at the center of the strain-broadened $M \rightarrow M-1$ ESR line from all the ions in the sample, there will be an NMR enhancement within the shell of influence of the ion with the deviation D whose resonant magnetic field is shifted by H' of Eq. (10). This effect is illustrated schematically in Fig. 1 in which the strain-broadened ESR line from all the ions is represented by the Gaussian function of width ΔH_M centered at the field H_0, and the ESR line from the ion with deviation D is represented by the Gaussian function of width ΔH centered at the field H_0+H'.

In accordance with part (ii) of our model of Sec. IIB, the NMR enhancement produced by the ion with the deviation D would be characterized by the negative of the first derivative of the Gaussian ESR line at H_0+H'; namely,

$$\mathcal{E}(H,H')=\frac{\mathcal{E}_{max}}{\Delta H}\,[H-(H_0+H')]\times e^{1/2}\exp\left(\frac{-[H-(H_0+H')]^2}{2\,\Delta H^2}\right), \tag{29}$$

where $\mathcal{E}_{max}$ is the magnitude of the maximum enhancement at the derivative peaks at $H=H_0+H'$

$\pm \Delta H$ (see the first-derivative line shape plotted by the dashed line in Fig. 1). Evaluation of Eq. (29) for $H = H_0$ and $H' = aD$ from Eq. (10) yields

$$\mathcal{E}(H = H_0, D) = -\frac{\mathcal{E}_{\max}}{\Delta H}(aD)\, e^{1/2} \exp\left(\frac{-a^2D^2}{2\,\Delta H^2}\right). \quad (30)$$

It is convenient to express the NMR enhancement of Eq. (30) in terms of quantities which can be obtained directly from DNP experimental data. Let $\mathcal{E}^T(H)$ be the dependence of the whole-sample NMR enhancement associated with the strain-broadened $M \rightarrow M-1$ ESR line. For an ideal case, $\mathcal{E}^T(H)$ would be proportional to the negative of the first derivative of the ESR line so that the width of $\mathcal{E}^T(H)$ is given by the ESR linewidth ΔH_M. We denote the magnitude of the maximum of $\mathcal{E}^T(H)$ by $\mathcal{E}_M$. The shape function for $\mathcal{E}^T(H)$ is characterized by the convolution of Eq. (14) and Eq. (29) [expressed in terms of D for H' based on Eq. (10)]; that is,

$$\mathcal{E}^T(H) = \int_{-\infty}^{\infty} \mathcal{E}(H, D)\, n(D, \Delta D, 0)\, dD. \quad (31)$$

This convolution yields

$$\mathcal{E}^T(H) = \frac{\mathcal{E}_M}{\Delta H_M}(H - H_0)\, e^{1/2} \exp\left(\frac{-(H-H_0)^2}{2\,\Delta H_M^2}\right), \quad (32)$$

with

$$\mathcal{E}_M = \mathcal{E}_{\max}\, \Delta H^2/(a^2\Delta D^2 + \Delta H^2), \quad (33)$$

$$\Delta H_M = (a^2\Delta D^2 + \Delta H^2)^{1/2}. \quad (34)$$

Substituting the values of $\mathcal{E}_{\max}$ and ΔH obtained from Eqs. (33) and (34) into Eq. (30) gives the following expression for the NMR enhancement within the shell of influence of the ion with the deviation D, at $H = H_0$:

$$\mathcal{E}(H = H_0, D) = \frac{-\mathcal{E}_M \Delta H_M^2 aD}{(\Delta H_M^2 - a^2\Delta D^2)^{3/2}} \times e^{1/2} \exp\left(\frac{-a^2D^2}{2(\Delta H_M^2 - a^2\Delta D^2)}\right). \quad (35)$$

The enhanced NMR signal $f_d(\nu, D)$ arising from the nuclear spins contained within the shell of influence of the ion with the deviation D is then given in terms of its thermal-equilibrium NMR line shape, $f(\nu, D)$ of Eq. (28), by

$$f_d(\nu, D) = f(\nu, D)\ \mathcal{E}(H = H_0, D). \quad (36)$$

The whole-sample NMR signal (arising from all shells) under DNP at $H = H_0$ is obtained by multiplying the enhanced signal from a given shell $f_d(\nu, D)$ by the distribution $n(D, \Delta D, 0)\, dD$ of Eq. (14) and integrating over D; namely,

$$f_d(\nu) = \int_{-\infty}^{\infty} f_d(\nu, D)\, n(D, \Delta D, 0)\, dD. \quad (37)$$

The evaluation of this integral yields the following NMR line shape:

$$f_d(\nu) = I_d\, \nu \exp\left(\frac{-\nu^2}{2\,\Delta\nu_d^2}\right), \quad (38)$$

with

$$I_d = \frac{-pA_m\mathcal{E}_M\, a\Delta D b\Delta Q \Delta H_M^2\, e^{1/2}}{(2\pi)^{1/2}[(\Delta\nu_m^2 + b^2\Delta Q^2)\,\Delta H_M^2 - (pa\Delta D b\Delta Q)^2]^{3/2}}, \quad (39)$$

$$\Delta\nu_d = \{\Delta\nu_m^2 + b^2\Delta Q^2[1 - (pa\Delta D/\Delta H_M)^2]\}^{1/2}. \quad (40)$$

[The calculations leading to Eqs. (38)–(40) can be modified to include cases in which the experimentally measured NMR enhancement from the whole sample $\mathcal{E}^T$ does not exactly follow the negative of the first-derivative ESR line shape due to, for example, an imperfect inhomogeneous broadening in the ESR line. In particular, when the experimental NMR enhancement $\mathcal{E}^T$ follows the negative of a Gaussian first-derivative line shape having a width $\Delta H'_M$ which is different from the ESR linewidth ΔH_M, it is sufficient to replace ΔH_M by $\Delta H'_M$ in Eqs. (39) and (40).]

It is seen from Eq. (38) that the NMR line shape under DNP represents the first derivative of a Gaussian function of derivative intensity I_d given by Eq. (39), and of width $\Delta\nu_d$ given by Eq. (40). In the following paragraphs we examine various possibilities for the over-all NMR quadrupole structures predicted by Eqs. (38)–(40) for a system with, for example, $S = \frac{3}{2}$ and $I = \frac{5}{2}$.

(i) We consider first the case in which the ESR and NMR strain effects are not at all correlated; that is, $p = 0$. From Eq. (39), all the NMR quadrupole component lines should vanish under DNP at the centers of all ESR fine-structure lines.

(ii) For microwave pumping power applied at the center of the $M = +\frac{1}{2} \rightarrow -\frac{1}{2}$ ESR fine-structure line (which is not strain broadened for $\vec{H} \parallel \vec{z}$), all the NMR quadrupole component lines should again vanish. In this case the coefficient a [$\equiv \mp(2M-1)/g_{\parallel}\beta_e$] in Eq. (39) is zero.

(iii) For pumping power applied at the centers of the strain-broadened $M = \pm\frac{3}{2} \rightarrow \pm\frac{1}{2}$ ESR fine-structure lines, the satellite NMR component lines ($m = \pm\frac{3}{2} \rightarrow \pm\frac{1}{2}$ and $m = \pm\frac{5}{2} \rightarrow \pm\frac{3}{2}$) exhibit nonvanishing NMR signals. However, the central NMR component line ($m = +\frac{1}{2} \rightarrow -\frac{1}{2}$) is always vanishing, since b [$\equiv \mp(2m-1)$] is zero for this NMR transition.

(iv) The low-frequency NMR satellite lines exhibit line shapes which are mirror images of the high-frequency NMR satellite lines under DNP at the centers of the $M = \pm\frac{3}{2} \rightarrow \pm\frac{1}{2}$ ESR lines. This results in a mirror symmetry with respect to the center of the NMR spectrum as shown in Figs. 2 and 3.

(v) For a given $m \rightarrow m-1$ NMR transition, the "phase" of the NMR line shape under DNP for a

negative sign of (pab) will be inverted (with respect to the baseline) from that for a positive sign of (pab) [compare Figs. 2(a) and 2(b) or Figs. 3(a) and 3(b)]. Since the signs of a and b depend on the absolute signs of the coupling constants $\mathfrak{D}$ and $\mathfrak{Q}$, respectively, the sign of p solely determines the respective phase of each NMR quadrupole component line. Thus by comparing the phase of the experimental NMR quadrupole structure with that predicted theoretically, the sign of p can be established.

(vi) The relative intensity of the inner $m = \pm\frac{3}{2} \rightarrow \pm\frac{1}{2}$ NMR satelline lines, $I_d(\pm\frac{3}{2} \rightarrow \pm\frac{1}{2})$, and outermost $m = \pm\frac{5}{2} \rightarrow \pm\frac{3}{2}$ satellite lines, $I_d(\pm\frac{5}{2} \rightarrow \pm\frac{3}{2})$, varies depending on the detailed nature of the ESR and NMR strain broadenings. To investigate this behavior, we calculate the ratio $|I_d(\pm\frac{3}{2} \rightarrow \pm\frac{1}{2})/I_d(\pm\frac{5}{2} \rightarrow \pm\frac{3}{2})|$ from Eq. (39) as

$$\left|\frac{I_d(\pm 3/2 \rightarrow \pm 1/2)}{I_d(\pm 5/2 \rightarrow \pm 3/2)}\right| = \frac{4}{5}\left(\frac{(\Delta\nu^2_{m=\pm 5/2}/\Delta\nu^2_{m=\pm 3/2}) + 16(\Delta Q/\Delta\nu_{m=\pm 3/2})^2[1-(pa\Delta D/\Delta H_M)^2]}{1+4(\Delta Q/\Delta\nu_{m=\pm 3/2})^2[1-(pa\Delta D/\Delta H_M)^2]}\right)^{3/2} . \tag{41}$$

Figure 4 shows a plot of Eq. (41) as a function of $\Delta Q/\Delta\nu_{m=\pm 3/2}$ for various values of $(pa\Delta D/\Delta H_M)$, where the ratio $(\Delta\nu^2_{m=\pm 5/2}/\Delta\nu^2_{m=\pm 3/2})$ is taken to be $(217/289)$.[32] It is seen in Fig. 4 that for large values of $\Delta Q/\Delta\nu_{m=\pm 3/2}$ and small values of $(pa\Delta D/\Delta H_M)$, the ratio of Eq. (41) may be greater than unity, in which case the intensities of the inner NMR satellite lines become greater than those of the outermost satellite lines, as illustrated in Fig. 2. For small values of $\Delta Q/\Delta\nu_{m=\pm 3/2}$ the ratio is less than unity, so that the outermost NMR satellite lines are of greater intensity than the inner NMR satellite lines, as shown in Fig. 3.

D. Reduction in NMR strain broadening under DNP

For the limiting case of an NMR enhancement $\mathcal{E}(H=H_0, D)$ in Eq. (36) equal to unity (that is, in the absence of DNP), the integral corresponding to Eq. (37) yields the following line-shape function:

$$f_0(\nu) = \frac{A_m}{(2\pi)^{1/2}\Delta\nu_0}\exp\left(\frac{-\nu^2}{2\Delta\nu_0^2}\right), \tag{42}$$

with

$$\Delta\nu_0 = (\Delta\nu_m^2 + b^2\Delta Q^2)^{1/2} . \tag{43}$$

This line shape should be consistent with the thermal-equilibrium NMR signal. In fact, Eq. (42) is the correct form for the thermal-equilibrium signal being a Gaussian function having the width $\Delta\nu_0$ of Eq. (43), which contains the intrinsic rigid-lattice nuclear-nuclear and electron-nuclear broadening $(\Delta\nu_m^2)$ as well as the strain broadening $(b^2\Delta Q^2)$.

As previously noted the DNP line shape $f_d(\nu)$ of Eq. (38) is proportional to the first derivative of a Gaussian function of width $\Delta\nu_d$ given by Eq. (40). We will refer to this width $\Delta\nu_d$ as the NMR linewidth under DNP. By comparing Eqs. (40) and (43), it is seen that the NMR linewidth under DNP, $\Delta\nu_d$, is predicted to be smaller than the width $\Delta\nu_0$ of the corresponding thermal-equilibrium signal. [For a schematic illustration of $\Delta\nu_d$ and $\Delta\nu_0$, compare the absorption NMR line shape under DNP shown by the dashed curve $f_d(\nu)$ in Fig. 5(a), and the first-derivative NMR line shape at thermal equilibrium shown by the solid curve $df_0(\nu)/d\nu$ in Fig. 5(b).] The amount of reduction in the NMR linewidth under DNP is determined by the factor $[1-(pa\Delta D/\Delta H_M)^2]$ in Eq. (40) multiplying the strain-broadening term $(b^2\Delta Q^2)$. This reduction factor is always less than 1 for nonzero p, and becomes increasingly important as the ESR strain broadening $(a\Delta D)$ becomes large. In the limit as $(pa\Delta D/\Delta H_M)^2$ approaches unity, the entire NMR strain-broadening contribution to the total NMR linewidth would be effectively eliminated.

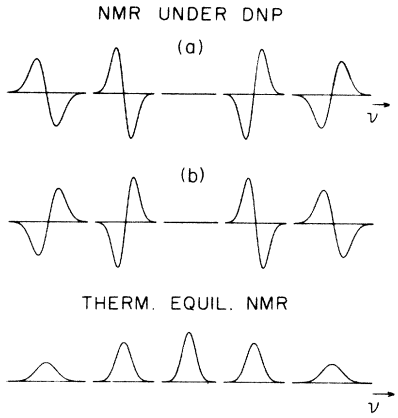

FIG. 2. NMR quadrupole absorption structures under DNP arising from the correlated ESR and NMR strain-broadening effect for the case of $|I_d(\pm\frac{3}{2} \leftrightarrow \pm\frac{1}{2})/I_d(\pm\frac{5}{2} \leftrightarrow \pm\frac{3}{2})| > 1$ in Eq. (41), and the corresponding thermal-equilibrium structure.

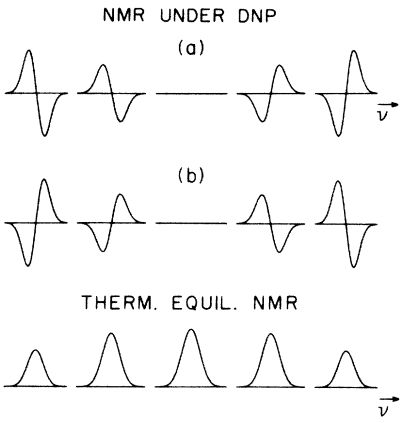

FIG. 3. NMR quadrupole absorption structures under DNP arising from the correlated ESR and NMR strain-broadening effect for the case of $|I_d(\pm\frac{3}{2}\leftrightarrow\pm\frac{1}{2})/I_d(\pm\frac{5}{2}\leftrightarrow\pm\frac{3}{2})|<1$ in Eq. (41), and the corresponding thermal-equilibrium structure.

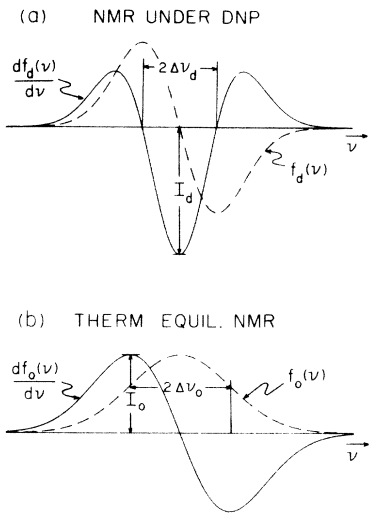

FIG. 5. Schematic illustration of the first-derivative peak intensity and linewidth of a strain-broadened NMR line (a) under DNP and (b) at thermal equilibrium.

E. Strain-induced enhancement $\mathcal{E}_s$ and the magnitude of p

The NMR signals under DNP and at thermal equilibrium can also be compared by considering the absolute intensities at the peaks of the first derivatives of the NMR line shapes of Eqs. (38) and (42). The most intense peak of the first-derivative NMR line shape under DNP occurs at the center of the NMR line with the intensity $|I_d|$ of Eq. (39) [see Fig. 5(a)]. The absolute intensity of the first-derivative peak of the thermal-equilibrium NMR signal of Eq. (42) [see Fig. 5(b)] is given by

$$|I_0| = \left| \frac{A_m e^{-1/2}}{(2\pi)^{1/2}(\Delta\nu_m^2 + b^2\Delta Q^2)} \right| . \tag{44}$$

We then introduce a new quantity, the "strain-induced enhancement," $\mathcal{E}_s$, defined as $\mathcal{E}_s \equiv |I_d|/|I_0|$. This ratio is obtained from Eqs. (39) and (44) as

$$\mathcal{E}_s = \left| \frac{p\,\mathcal{E}_M\, a\,\Delta D\, b\,\Delta Q\,\Delta H_M^2(\Delta\nu_m^2 + b^2\Delta Q^2)\,(2.71)}{[(\Delta\nu_m^2 + b^2\Delta Q^2)\Delta H_M^2 - (pa\Delta Db\Delta Q)^2]^{3/2}} \right| . \tag{45}$$

All of the quantities in the above expression for $\mathcal{E}_s$, with the exception of the correlation parameter p, can be obtained from ESR, NMR, and DNP experimental data. Thus by comparing the theoretical value of $\mathcal{E}_s$ of Eq. (45) with the corresponding experimental value, the magnitude of the correlation parameter p can be evaluated.

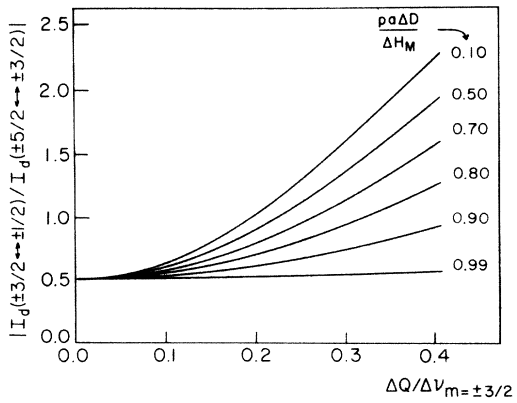

FIG. 4. Plot of Eq. (41) as a function of $\Delta Q/\Delta\nu_{m=\pm3/2}$ for various values of $pa\Delta D/\Delta H_M$.

F. Inclusion of additional NMR substructures

It has been assumed in the preceding calculations that each NMR quadrupole component line can be described by a single Gaussian line-shape function. We now consider the case in which the NMR component lines exhibit additional substructures arising, for example, from a nearest-neighbor nuclear dipole interaction as in the case of ruby.[33] To treat this in a simple manner, the possible crystalline strain effects on the coupling constant giving rise to the substructure will be neglected, since they would be very small compared to the strain effects on the NMR quadrupole coupling constant.

We consider that the $m \leftrightarrow m-1$ NMR quadrupole component line consists of several substructure component lines each of which possesses a Gaussian line shape. Hence, the ith subcomponent line can be expressed as

$$g(\nu-\nu_i) = \frac{A_m^i}{(2\pi)^{1/2}\Delta\nu_m^i} \exp\left(\frac{-(\nu-\nu_i)^2}{2\,\Delta\nu_m^{i2}}\right), \tag{46}$$

where A_m^i is the relative NMR intensity, and $\Delta\nu_m^i$ is the intrinsic linewidth of this subcomponent line. For the nuclear spin with the deviation Q in its quadrupole coupling constant, the NMR frequency of each of the subcomponent lines in the $m \leftrightarrow m-1$ NMR quadrupole line is shifted by the same amount ν' given by Eq. (12). Thus the over-all NMR line shape for the $m \leftrightarrow m-1$ NMR quadrupole line is given by

$$g(\nu-\nu') = \sum_i \frac{A_m^i}{(2\pi)^{1/2}\Delta\nu_m^i} \exp\left(\frac{-[\nu-(\nu_i+\nu')]^2}{2\,\Delta\nu_m^{i2}}\right) . \tag{47}$$

To determine the shape function $f_d(\nu)$ for the $m \leftrightarrow m-1$ NMR quadrupole line from the whole sample under DNP, we use Eq. (47) in place of Eq. (23) in the calculations leading to Eq. (38). This results in the following expression:

$$f_d(\nu) = \sum_i I_d^i(\nu-\nu_i) \exp\left(\frac{-(\nu-\nu_i)^2}{2\,\Delta\nu_d^{i2}}\right) , \tag{48}$$

with

$$I_d^i = \frac{-pA_m^i \mathcal{E}_M a\,\Delta D\, b\,\Delta Q\,\Delta H_M^2 e^{1/2}}{(2\pi)^{1/2}[(\Delta\nu_m^{i2}+b^2\Delta Q^2)\Delta H_M^2 - (pa\Delta D b\Delta Q)^2]^{3/2}} , \tag{49}$$

$$\Delta\nu_d^i = \{\Delta\nu_m^{i2} + b^2\Delta Q^2[1-(pa\Delta D/\Delta H_M)^2]\}^{1/2} . \tag{50}$$

The corresponding thermal-equilibrium NMR line shape for the whole sample, including strain broadening, is

$$f_0(\nu) = \sum_i \frac{A_m^i}{(2\pi)^{1/2}\Delta\nu_0^i} \exp\left(\frac{-(\nu-\nu_i)^2}{2\,\Delta\nu_0^{i2}}\right) , \tag{51}$$

with

$$\Delta\nu_0^i = (\Delta\nu_m^{i2} + b^2\Delta Q^2)^{1/2} . \tag{52}$$

By comparing Eqs. (48) and (51), the following can be concluded: (i) All the subcomponent lines contained within the central $m = +\frac{1}{2} \leftrightarrow -\frac{1}{2}$ quadrupole transition vanish under DNP. (ii) The shape of each subcomponent line in the satellite quadrupole transitions becomes proportional to either the positive or negative of the first derivative of the thermal-equilibrium Gaussian line shape, and the width of this Gaussian line shape is reduced from that of the thermal-equilibrium signal by the factor $[1-(pa\Delta D/\Delta H_M)^2]$. (iii) Since the over-all line shape of each satellite quadrupole line is characterized by the sum of the individual subcomponent lines, the over-all line shape will be similar to either the positive or negative of the first derivative of its thermal-equilibrium line shape. However, owing to the reduction of linewidth of each subcomponent line under DNP, a better resolution of the NMR substructures may be achieved in the NMR absorption spectra under DNP as compared to the first-derivative thermal-equilibrium NMR spectra. (iv) The phases of the low-frequency satellite quadrupole component lines will be opposite to those of the high-frequency satellite component lines; thus, the entire NMR spectrum under DNP will exhibit a mirror symmetry with respect to the center of the spectrum, if the thermal-equilibrium spectrum displays a mirror symmetry.

If the relative intensities and frequency spacings of the NMR subcomponent lines are known, it is possible in principle to derive, for the purpose of determining the magnitude of p, an analytic expression for the strain-induced enhancement $\mathcal{E}_s$ corresponding to Eq. (45). However, this procedure may be unnecessarily complicated. As an alternative, one can determine the magnitude of p by finding the p value which gives the best-fit theoretical NMR line shapes and intensities calculated from Eq. (48) to the experimentally observed data. In fact, this latter procedure will be adopted in analyzing the experimental data obtained from ruby crystals investigated in the present work.

III. EXPERIMENTAL

A. Instrumentation and samples

The experiments were performed using a Varian V-4500 X-band ESR spectrometer in conjunction with a Robinson-type NMR detector constructed in this laboratory. Microwave power was supplied by a Varian V-58C fixed-frequency klystron which delivered a maximum of approximately 150 mW power to a rectangular cavity operated in the TE_{012} mode. A magnetic field was provided by a Varian 12-in. rotatable magnet with a field-regulated power supply.

Four ruby samples with different Cr^{3+}-ion concentrations were investigated in this work. Two of the samples were obtained from the Linde Division of Union Carbide Corp. with specified Cr^{3+}-ion concentrations. The Cr^{3+}-ion concentrations of the remaining samples, which were obtained from the Adolph Mellor Co., were determined by ESR intensity measurements using the Linde samples as a reference. All of the samples were grown by the Verneuil (flame-fusion) method and were of laser quality.

The samples were cut into rectangular parallelepipeds of dimensions approximately $10\times2\times2$ mm with the c axis ($\vec{c}$) of the crystal parallel to one of the short edges of the sample. Each sample was encircled with 6 to 15 turns of fine copper wire (No. 34) forming an NMR rf coil with its axis perpendicular to both the c axis of the crystal and the longest dimension of the sample. The crystal and rf coil were secured with epoxy cement to the end of a quartz tube which served as a holder for the coaxial cable linking the probe to the Robinson NMR oscillator.

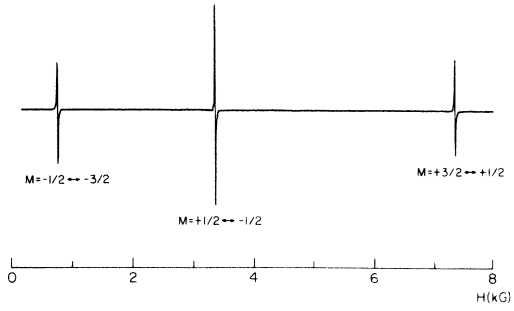

FIG. 6. Cr^{3+} ESR spectrum in the ruby sample with 0.04-wt% Cr_2O_3 concentration for $\vec{H} \parallel \vec{c}$ at a microwave frequency of 9.1 GHz at 77 °K.

For the DNP measurements, all of which were conducted at liquid-nitrogen temperatures, the samples were lowered into a quartz Dewar centered in the microwave cavity. The crystals were aligned with respect to the external field $\vec{H}$ by making use of the strong angular dependence of the Cr^{3+} ESR fine-structure lines. After adjusting the external field $\vec{H}$ to the position desired for DNP on a given ESR fine-structure line, maximum microwave power was delivered to the cavity to saturate this portion of the line. The rf frequency of the Robinson NMR oscillator was then scanned through the proper frequency range by means of a motor-driven variable capacitor connected in parallel with the oscillator tank circuit. Recorder traces of the first-derivative NMR line shapes were obtained using a field modulation of 200 Hz.

B. Experimental results and analyses

1. ESR *experiments*. Figure 6 displays the Cr^{3+} ESR spectrum observed in ruby for $\vec{H} \parallel \vec{c}$ at a microwave frequency of 9.1 GHz. Since the absolute sign of the fine-structure splitting constant $\mathfrak{D}$ of the Cr^{3+} ions (with effective spin $S=\frac{3}{2}$) in ruby is negative,[34] the three ESR fine-structure lines situated at low, intermediate, and high fields correspond to the $M=-\frac{1}{2} \leftrightarrow -\frac{3}{2}$, $M=+\frac{1}{2} \leftrightarrow -\frac{1}{2}$, and $M=+\frac{3}{2} \leftrightarrow +\frac{1}{2}$ ESR transitions, respectively. The shapes of the lines were observed to be approximately Gaussian in each of the four samples.

To determine experimentally the width ΔD representing the Cr^{3+} strain broadening, we first determined the linewidth ΔH_M for each $M \leftrightarrow M-1$ ESR fine-structure line by measuring the half-separation between the two peaks in the first-derivative ESR line. The widths of the $M=\pm\frac{3}{2} \leftrightarrow \pm\frac{1}{2}$ satellite lines $\Delta H_{M=\pm 3/2}$ were observed to be larger than the width of the central $M=+\frac{1}{2} \leftrightarrow -\frac{1}{2}$ ESR line $\Delta H_{M=+1/2}$ in each sample, indicating that the $M=\pm\frac{3}{2} \leftrightarrow \pm\frac{1}{2}$ satellite lines are strain broadened.

In order to calculate the strain broadening, we assumed that the ESR linewidths in an unstrained or perfect crystal arise from the hyperfine interactions of the Cr^{3+} ions with the surrounding nuclear spins and from the rigid-lattice dipole-dipole interactions between the Cr^{3+} ions. The relative size of the hyperfine and dipolar contributions to the linewidths was determined as follows. Figure 7 shows the experimental second moments of the central $M=+\frac{1}{2} \leftrightarrow -\frac{1}{2}$ lines (darkened circles) and satellite $M=\pm\frac{3}{2} \leftrightarrow \pm\frac{1}{2}$ lines (open circles) plotted as a function of the wt% Cr_2O_3 in the samples. The experimental second moments were taken to be the squares of the widths of the lines based on the Gaussian ESR line shapes.[25] The increase in the second moment of the central ESR line with Cr^{3+}-ion concentration was fit with a straight line using the method of least squares. With this fit the hyperfine contribution to the second moment of the central line was assumed to be given by the extrapolated value of the second moment for the vanishing Cr^{3+}-ion concentration, 28.1 G^2. The difference between this second moment and the total second moment of the central line for a given concentration was taken to be the dipolar contribution to the second moment of this line.

The dipolar contribution to the second moments of the satellite $M=\pm\frac{3}{2} \leftrightarrow \pm\frac{1}{2}$ lines has been shown theoretically[35,36] to be smaller by a factor of 69/81 than its contribution to the second moment of the central $M=+\frac{1}{2} \leftrightarrow -\frac{1}{2}$ line for $S=\frac{3}{2}$. The hyperfine interactions, however, theoretically contribute the same second moment to both the satellite and central ESR lines.[37] Hence, the second moments of the satellite lines in a perfect crystal were calculated by multiplying the dipolar second moment of the central ESR line in a given sample by 69/81 and adding this result to the second moment due to the hyperfine interactions. The strain-broadening contribution, described by the width ΔD, was evaluated by comparing the second moment determined

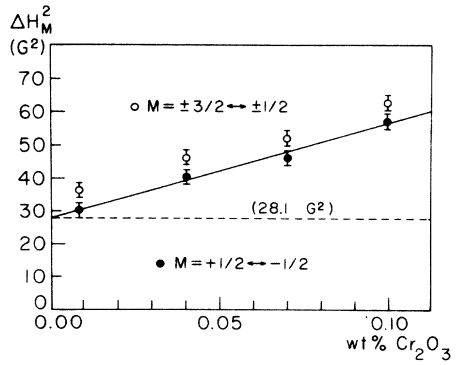

FIG. 7. Measured second moments of the Cr^{3+} ESR fine-structure lines in the ruby samples versus the sample wt% Cr_2O_3.

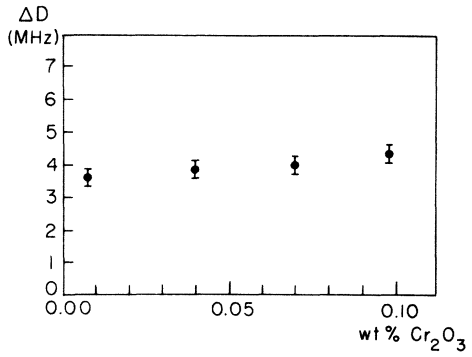

FIG. 8. Cr^{3+} ESR strain-broadening widths ΔD measured for the ruby samples versus the sample wt% Cr_2O_3 (see also Table I).

for the perfect crystal with the experimental total second moment of the satellite lines. The values of ΔD obtained in this manner for the four crystals are shown in Fig. 8 and Table I.

2. NMR *experiments*. The experimental first-derivative ^{27}Al NMR spectrum in ruby at thermal equilibrium ($\vec{H} \parallel \vec{c}$) is shown in Fig. 9(a), and the corresponding absorption spectrum obtained by numerical integration is shown in Fig. 9(b). The partially resolved substructure on each quadrupole component line arises from the nearest-neighbor ^{27}Al nuclear dipolar interaction which gives rise to the theoretical line spectrum of Fig. 9(c).[33] Because of this substructure, the second moments of the quadrupole components were obtained directly from the mean-square frequency deviations of the observed lines.

A total of four first-derivative traces were recorded for each of the five quadrupole component lines of a given sample. These first-derivative traces were calibrated by means of a frequency marker at intervals of 0.5 kHz. Approximately eighty calibration points were recorded on each resonance line, care being taken to extend the calibration points into the wings of the line to establish the first-derivative NMR baseline. Each first-derivative NMR line was then integrated numerically to determine the second moment.

The experimentally measured second moments of the various NMR quadrupole component lines $\Delta\nu_0^2$ are shown in Fig. 10. It is seen that for a given sample, the second moments decrease progressively from the central to outermost satellite lines. This decrease, however, does not exclude strain-broadening contributions to the satellite lines, since as previously noted,[32] the rigid-lattice nuclear-nuclear dipolar interactions give rise to second moments in the ratio 217 : 289 : 321 : 289 : 217 for the five NMR quadrupole component lines for $I = \frac{5}{2}$. The nuclear-electron dipolar interactions between the Cr^{3+} ions and ^{27}Al nuclear spins contribute the same second moment to all NMR lines.

The relative amount of nuclear-nuclear and nuclear-electron dipolar broadening was determined in a manner similar to that described for the Cr^{3+} ESR lines. The least-squares fit of a straight line to the measured second moments of the central NMR line resulted in a value of 9.3 kHz^2 at the vanishing Cr^{3+}-ion concentration, which was taken to be the nuclear-nuclear dipolar contribution to the total second moment of this line. For the satellite NMR lines the nuclear-nuclear dipolar contribution was obtained by multiplying 9.3 kHz^2 by $\frac{217}{321}$ and $\frac{289}{321}$, respectively, for the $m = \pm\frac{5}{2} \leftrightarrow \pm\frac{3}{2}$ and $m = \pm\frac{3}{2} \leftrightarrow \pm\frac{1}{2}$ component lines.

The intrinsic, rigid-lattice second moments of the $m \leftrightarrow m-1$ satellite lines in an unstrained crystal, $\Delta\nu_m^2$, were determined by combining the nuclear-nuclear and nuclear-electron dipolar second moments, where the latter was obtained from the central NMR line at a given concentration. These second moments, $\Delta\nu_m^2$, are shown for the various samples in Table I. The width ΔQ representing the strain broadening was then evaluated from the difference between $\Delta\nu_m^2$ and the observed total second moments of the satellite lines. The average of the four values of ΔQ obtained for the four crystals are displayed in Fig. 11 and Table I.

3. DNP *experiments*. The dynamic-nuclear-polarization experiments consisted in investigating

TABLE I. Experimentally measured values for the Cr^{3+} ESR strain broadening ΔD, the intrinsic rigid-lattice second moments for the various ^{27}Al NMR quadrupole component lines $\Delta\nu_m^2$, the ^{27}Al NMR strain broadening ΔQ, the width of the NMR enhancement curve associated with the $M = +\frac{3}{2} \leftrightarrow +\frac{1}{2}$ Cr^{3+} ESR line $\Delta H'_M$, the maximum NMR enhancement δ_M, and the correlation parameter p in the four ruby samples.

Ruby samples (wt% Cr_2O_3)	ΔD (MHz)	$\Delta\nu^2_{m=\pm1/2}$	$\Delta\nu^2_{m=\pm3/2}$ (kHz^2)	$\Delta\nu^2_{m=\pm5/2}$	ΔQ (kHz)	$\Delta H'_M$ (G)	δ_M $M = +\frac{3}{2} \leftrightarrow +\frac{1}{2}$	p
0.008	3.6	9.5	8.6	6.5	0.17	6.5	40	0.5
0.040	3.9	10.1	9.2	7.0	0.18	8.8	28	0.5
0.070	4.0	10.6	9.7	7.6	0.20	10.2	24	0.6
0.099	4.4	11.2	10.3	8.1	0.24	13.5	17	0.7

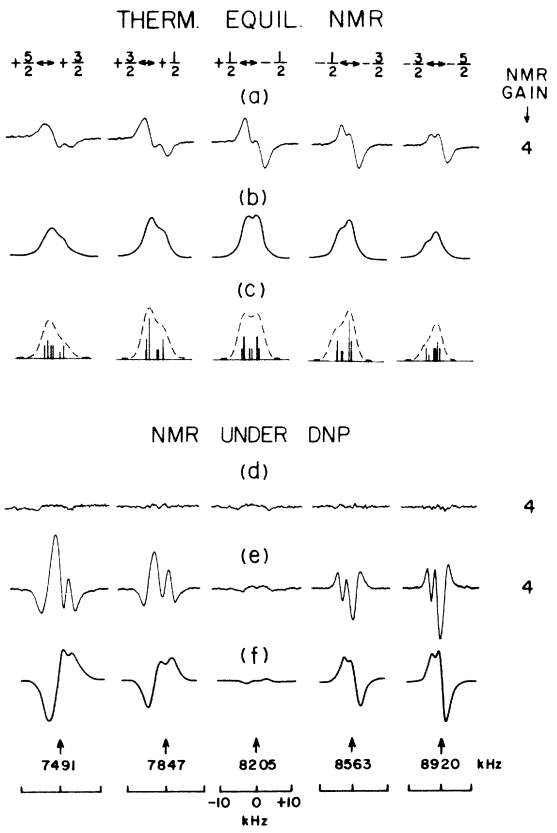

FIG. 9. Thermal-equilibrium ^{27}Al NMR quadrupole structures and the corresponding NMR quadrupole structures under DNP for the ruby sample with 0.04-wt% Cr_2O_3 concentration at 77 °K. All the spectra in this figure, except that shown in part (d), are plotted based on the frequency scale shown in the bottom of the figure.

the behavior of the ^{27}Al NMR spectra by applying saturating microwave pumping power at various parts of the Cr^{3+} ESR spectrum with $\vec{H} \parallel \vec{c}$. However, the resonance field of the $M = -\frac{1}{2} \leftrightarrow -\frac{3}{2}$ Cr^{3+} ESR line was so low (approximately 800 G as seen in Fig. 6) that the ^{27}Al NMR frequency at this magnetic field fell outside the frequency range of our Robinson NMR detector. Consequently, the $M = -\frac{1}{2} \leftrightarrow -\frac{3}{2}$ ESR line was not suitable for our DNP experiments.

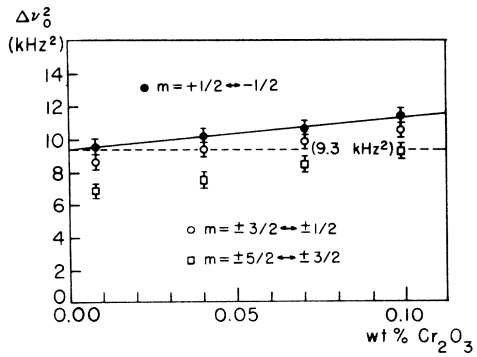

FIG. 10. Measured second moments of the ^{27}Al NMR quadrupole component lines in the ruby samples versus the sample wt% Cr_2O_3.

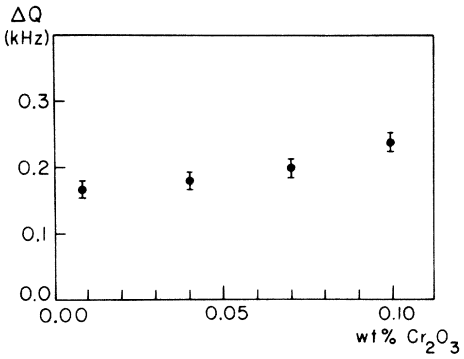

FIG. 11. NMR strain-broadening widths ΔQ measured for the ruby samples versus the sample wt% Cr_2O_3 (see also Table I).

It was found that except for the center portion of each Cr^{3+} fine-structure line, the NMR spectra observed under DNP were either positively or negatively polarized, with the shape of the ^{27}Al quadrupole structure remaining the same as that of the thermal-equilibrium signals. Figure 12 shows the NMR enhancements $\mathcal{E}^T(H)$ obtained from saturating various parts on the $M = +\frac{3}{2} \leftrightarrow +\frac{1}{2}$ ESR line in the sample with 0.04-wt% Cr_2O_3 concentration. Each data point represents the average NMR enhancement for the five quadrupole component lines. The solid curve in Fig. 12 shows the experimental first-derivative of the $M = +\frac{3}{2} \leftrightarrow +\frac{1}{2}$ ESR line, and the dashed curve represents an approximation to

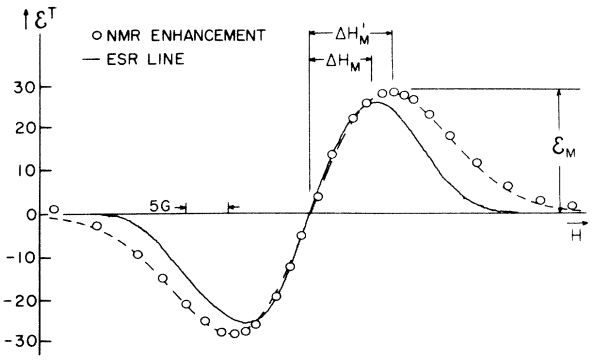

FIG. 12. NMR enhancements $\mathcal{E}^T$ at various points on the $M = +\frac{3}{2} \leftrightarrow +\frac{1}{2}$ Cr^{3+} ESR line in the ruby sample with 0.04-wt% Cr_2O_3 concentration for $\vec{H} \parallel \vec{c}$ at 77 °K.

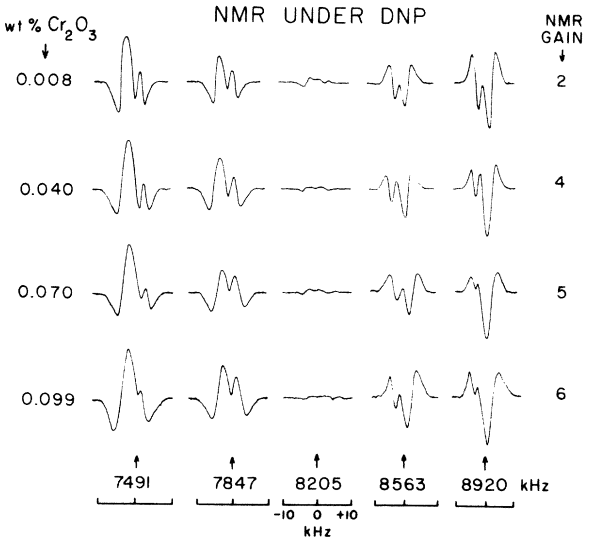

FIG. 13. First-derivative ^{27}Al NMR quadrupole structures under DNP at the center of the $M=+\frac{3}{2} \leftrightarrow +\frac{1}{2}$ Cr^{3+} fine-structure line in the various ruby samples for $\vec{H} \| \vec{c}$ at 77 °K.

the measured NMR enhancements by the first derivative of a Gaussian function.

It is seen that the width $\Delta H'_M$ of the enhancement curve $\mathcal{S}^T(H)$ is noticeably larger than the corresponding ESR linewidth ΔH_M, although it is approximately Gaussian in shape. This behavior was observed in all samples under DNP on the $M=+\frac{3}{2} \rightarrow +\frac{1}{2}$ ESR line as well as on the central $M=+\frac{1}{2} \rightarrow -\frac{1}{2}$ ESR line. It is believed that the departure of $\mathcal{S}^T(H)$ from the ESR line shape arises from the possibility that the ESR lines are partially homogeneously broadened owing to the electron spin-spin interactions. The experimental width $\Delta H'_M$ and the maximum value of $\mathcal{S}^T(H)$, $\mathcal{S}_M$, for the various samples are listed in Table I.

To investigate the correlated ESR and NMR strain effect, the detailed line shapes of the five ^{27}Al NMR component lines were investigated for each sample by saturating the center portions of the $M=+\frac{1}{2} \rightarrow -\frac{1}{2}$ and $M=+\frac{3}{2} \rightarrow +\frac{1}{2}$ ESR lines. The results obtained from the sample with 0.04-wt% Cr_2O_3 are displayed in Fig. 9 along with the thermal-equilibrium NMR data for direct comparison purposes. As expected, under DNP at the center of the strain-free $M=+\frac{1}{2} \rightarrow -\frac{1}{2}$ ESR line, no resonance lines were observed which could be clearly distinguished from the noise level [see Fig. 9(d)]. However, the NMR spectrum under DNP at the center of the strain-broadened $M=+\frac{3}{2} \rightarrow +\frac{1}{2}$ ESR line exhibited the structure of Fig. 9(e). The corresponding absorption line shapes obtained by numerical integration of the first-derivative line shapes of Fig. 9(e) are shown in Fig. 9(f). It is noted that the same NMR spectrometer gain was used for the three first-derivative spectra of Figs. 9(a), 9(d), and 9(e).

The shapes of the NMR signals under DNP for the other three samples were qualitatively similar to those observed for the 0.04-wt% Cr_2O_3 sample. That is, under DNP at the center of the strain-free $M=+\frac{1}{2} \rightarrow -\frac{1}{2}$ ESR line no NMR signals were detected, while at the center of the $M=+\frac{3}{2} \rightarrow +\frac{1}{2}$ ESR line, NMR quadrupole structures similar to that shown in Fig. 9(e) were observed. These structures are displayed in Fig. 13, in which we include the data from the sample with 0.04-wt% Cr_2O_3 concentration for comparison purposes. The important difference between the crystals was the NMR intensities or enhancements of the ^{27}Al quadrupole structures under DNP. This intensity variation from sample to sample can be seen in terms of the relative NMR spectrometer gain employed in taking each spectrum in Fig. 13.

It should be noted from Figs. 9 and 13 that (i) the central $m=+\frac{1}{2} \rightarrow -\frac{1}{2}$ NMR transition is nearly vanishing in the noise level, (ii) the shape of each NMR satellite component line approximates either the positive or negative first derivative of the corresponding thermal-equilibrium line shape [compare Figs. 9(e) and 9(a)], (iii) the over-all NMR absorption quadrupole structure obtained by the numerical integration of the first-derivative lines [Fig. 9(f)] has a mirror symmetry with respect to the center of the NMR spectrum, and (iv) the NMR intensities of the outermost $m=\pm\frac{5}{2} \rightarrow \pm\frac{3}{2}$ NMR satellite lines are greater than those of the inner $m=\pm\frac{3}{2} \rightarrow \pm\frac{1}{2}$ satellite lines. These observations are consistent with the NMR quadrupole structure predicted on the basis of the correlated ESR and NMR strain-broadening effect discussed in Sec. II.

To determine the absolute sign of p, we compared the observed phases of the low- and high-frequency ^{27}Al NMR satellite lines under DNP with those predicted on the basis of Eqs. (48) and (49) in which the phase of a given NMR component line is determined by the net sign of (pab). Since the absolute sign of the ^{27}Al nuclear quadrupole coupling constant $\mathcal{Q}$ in ruby is known to be positive,[33] the sign of b, defined by Eq. (13), is negative for the low-frequency NMR satellite lines and positive for the high-frequency NMR satellite lines. The sign of a, defined by Eq. (11), is positive for the $M=+\frac{3}{2} \rightarrow +\frac{1}{2}$ ESR fine-structure line, since the absolute sign of the Cr^{3+} ESR fine-structure constant $\mathcal{D}$ in ruby is negative.[34] Hence, to obtain agreement with the observed phases of the experimental spectra under DNP shown in Fig. 13, the sign of p should be positive for all crystals.

The magnitude of p in each crystal was established from the best-fit theoretical NMR intensities under DNP to the experimental data. That is,

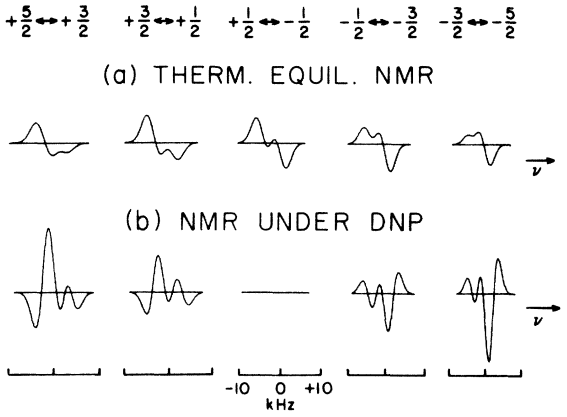

FIG. 14. Theoretical first-derivative ^{27}Al NMR quadrupole structures for the ruby sample with 0.04-wt% Cr_2O_3 concentration for $\vec{H} \| \vec{c}$ (a) at thermal equilibrium and (b) under DNP.

using the experimentally measured parameters ΔD, ΔQ, $\Delta\nu_m$, $\Delta H'_M$, and $\mathcal{E}_M$ listed in Table I, the theoretical NMR structures were fit to the experimental signals solely by varying the magnitude of p. We illustrate this fitting procedure for the sample with 0.04-wt% Cr_2O_3 in Fig. 14.

Figure 14(a) shows, for reference, the first-derivative thermal-equilibrium NMR spectrum $df_0(\nu)/d\nu$ calculated from Eq. (51) including the NMR strain broadening ΔQ for this sample. The height or intensity of this thermal-equilibrium spectrum was first adjusted by means of a vertical scaling factor (gain factor) to fit the actual intensity of the experimentally observed thermal-equilibrium signal of Fig. 9(a). The theoretical first-derivative NMR spectrum under DNP $df_d(\nu)/d\nu$ was then calculated from Eq. (48), using the same vertical gain factor, since the same NMR spectrometer gain was used to obtain both the thermal-equilibrium spectrum of Fig. 9(a) and the spectrum under DNP of Fig. 9(e). The intensity

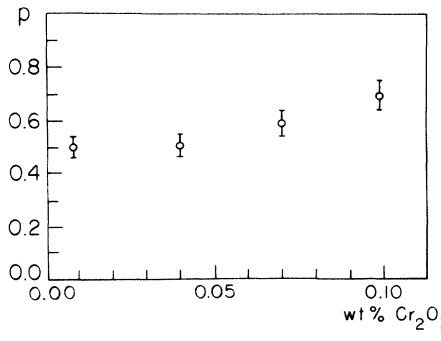

FIG. 15. Correlation parameter p obtained for the various ruby samples versus the sample wt% Cr_2O_3 (see also Table I).

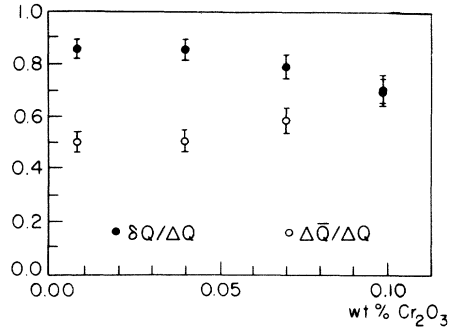

FIG. 16. Values of $\delta Q/\Delta Q$ and $\Delta\bar{Q}/\Delta Q$ determined from p using Eqs. (21) and (22) versus the sample wt% Cr_2O_3.

of the theoretical NMR spectrum under DNP was adjusted using different p values to achieve the best fit to the experimentally observed NMR intensity under DNP of Fig. 9(e). The best-fit theoretical spectrum was obtained with $p = 0.5$ for the sample with 0.04-wt% Cr_2O_3 concentration and is shown in Fig. 14(b). Employing this fitting procedure for the other samples, we obtained the values of p listed in Table I and plotted in Fig. 15. The magnitude of p appears to increase as the Cr_2O_3 concentration increases.

The contributions to the strain broadening in the ^{27}Al NMR lines due to short-range strain effects, represented by $\delta Q/\Delta Q$, and due to long-range strain effects, represented by $\Delta\bar{Q}/\Delta Q$, were calculated from p in each crystal using Eqs. (21) and (22). These results for the four samples are plotted in Fig. 16.

IV. DISCUSSIONS

It is seen that the experimental data of the ^{27}Al NMR quadrupole structures under DNP at the centers of the Cr^{3+} ESR fine-structure lines for $\vec{H} \| \vec{c}$ are in general agreement with the theoretical results predicted on the basis of the correlated ESR and NMR strain-broadening effect. However, we note one apparent discrepancy between the theory and experiment which is concerned with the central $m = +\frac{1}{2} \leftrightarrow -\frac{1}{2}$ NMR quadrupole component line. In the experimental spectra of Fig. 13, the central NMR quadrupole component line appears to show a nonvanishing signal in the various samples, while theoretically it should be vanishing. This discrepancy may be due to the following two DNP effects which have been previously investigated.

The first is associated with the broadening of ESR and NMR lines arising from inhomogeneities in the external magnetic field employed in the DNP experiments.[38,39] Owing to this line-broadening mechanism, DNP at the center of an ESR line causes all the NMR quadrupole component lines,

including the central $m = +\frac{1}{2} \rightarrow -\frac{1}{2}$ NMR line, to show absorption signals roughly proportional to the first-derivative line shapes of the thermal-equilibrium signals. The over-all NMR absorption spectrum will therefore lack mirror symmetry with respect to the center of the spectrum. In addition, the relative intensities of the various quadrupole NMR component lines under DNP would be the same as those observed for the thermal-equilibrium signals; that is, 5:8:9:8:5 for $I = \frac{5}{2}$. In view of the definite mirror symmetry [see Fig. 9(f)] and larger NMR intensities observed for the outermost NMR satellite lines in the experimental absorption spectra, the effect of magnetic field inhomogeneities on the satellite NMR lines in certainly unimportant. It is probable, however, that there is a small field-inhomogeneity effect present which is just strong enough to be responsible for the observed weak signals from the central NMR quadrupole component lines in Fig. 13.

The second possible cause of the central NMR lines under DNP is the Δ^2/δ effect,[40] where Δ and δ are the electron and nuclear Boltzmann factors, respectively. This effect is associated with the second-order differences in the nuclear-spin populations produced under DNP at the center of an ESR line which is inhomogeneously broadened by unresolved hyperfine interactions. For this effect, a given NMR satellite component line under DNP will be wholly positively or wholly negatively enhanced with the same shape as the thermal-equilibrium signal. The central NMR component line should vanish, unless there is substructure associated with it as in the case of ruby. Calculations have shown that the shape of the central ^{27}Al NMR component line in ruby associated with the Δ^2/δ effect would be similar to the first-derivative line shape of its thermal-equilibrium signal.[41] Although the Δ^2/δ effect is expected to be very weak in the ruby systems,[42] it cannot be completely ruled out as a possible source of the weak signals observed for the central ^{27}Al NMR lines under DNP.

It should be mentioned that unusual NMR quadrupole structures can also be produced under DNP at the center of an ESR line owing to ESR and NMR symmetry-axis variations (the c-axis variation effect).[39,43] Although this effect will produce a mirror symmetry in the absorption line shapes of the NMR quadrupole structure under DNP, it should vanish when the external magnetic field $\vec{H}$ is applied parallel to the symmetry axis in the case of axial symmetry. In fact, the reason that both the theoretical and experimental investigations of the correlated strain effect in the present work are confined to the case $\vec{H} \parallel \vec{c}$, is to avoid the c-axis variation effect, since at other crystal orientations it could mask the correlated strain effect.

The absolute sign of the correlation parameter p is found to be positive in all the ruby crystals investigated. This means that the ESR fine-structure constant of a given Cr^{3+} ion and the average NMR quadrupole coupling constant of the ^{27}Al nuclear spins in the shell of influence of this ion are deviated simultaneously to values which are greater or less in magnitude than the perfect-crystal values. In the ruby lattice, the Cr^{3+} ion is substitutional for the Al^{3+} ion, and the equivalence of the Cr^{3+} ion and ^{27}Al nuclear-spin sites may have a bearing on the observed positive sign of the correlation parameter. Obviously, to understand the exact origin and significance of the sign of the correlation parameter p, it is essential to obtain detailed knowledge concerning the strain mechanisms responsible for the observed correlated ESR and NMR strain-broadening effect in DNP.

As seen from Fig. 15, the observed magnitudes of the correlation parameter p range from 0.5 to 0.7 and appear to increase with increasing Cr^{3+}-ion concentration. Two possibilities can be considered for this increasing trend. When the Cr^{3+}-ion concentration is increased, the average diameter of the shells of influence of the ions is reduced. Hence, if one assumes that the correlated ESR and NMR strain effect has a definite range, the correlation within a given shell of influence would in effect increase as the diameter of the shell is reduced approaching the range of the correlation. The second consideration is that the Cr^{3+} impurity ions themselves may introduce strains in the crystal which become part of the total strain mechanisms responsible for the correlation. If this is the case, the correlation would also increase with the Cr^{3+}-ion concentration.

One might attempt to consider the behavior of p in the limiting cases of very high or very low Cr^{3+}-ion concentrations, outside the range of concentrations investigated in this work. It should be remembered, however, that if the paramagnetic ion concentration is very high or very low, other effects may become important which would invalidate the assumptions employed in the theoretical model and/or make unfavorable the detection of the correlated strain effect. For example, at very high concentrations the electron spin-spin interactions would cause the ESR fine-structure lines to become primarily homogeneously broadened,[35] and at very low concentrations the Solid Effect would be too weak to produce sizable NMR enhancements throughout the whole crystal.

According to the theoretical predictions of Sec. II F, the dipolar substructure on each ^{27}Al quadrupole component line should exhibit a better resolution owing to the linewidth reduction under DNP. In comparing the first-derivative thermal-equi-

librium NMR spectrum of Fig. 9(a) and the absorption spectrum under DNP of Fig. 9(f), such an improvement in resolution is not noticeable. This result is not surprising in view of the fact that for the ruby samples investigated, the value of $(pa\Delta D/\Delta H'_M)^2$ in the linewidth reduction factor is negligibly small; for example, for the sample with 0.04-wt% Cr_2O_3, $(pa\Delta D/\Delta H'_M)^2$ is approximately 0.03.

The theoretical treatment of the correlated strain effect discussed in this paper has been restricted to the case of strain-broadened ESR fine-structure and NMR quadrupole-structure lines. Employing the same method, one can also treat the case of ESR lines broadened by variations in the g value or hyperfine coupling constant, and NMR lines broadened by variations in the nuclear dipolar-structure (e.g., Pake doublet) coupling constant. It is expected that the results similar to Eqs. (38)–(40) should be obtained for the line shape of each NMR component line associated with the correlated ESR and NMR strain-broadening effect in DNP. One should also note that in the theoretical model, the NMR enhancement under DNP is assumed to arise from the simple Solid Effect associated with inhomogeneously broadened ESR line. If there are other DNP processes important for the system under investigation, they can readily be taken into account in the theoretical model.

V. SUMMARY AND CONCLUSIONS

Quantitative theoretical and experimental investigations have been made of the behavior of strain-broadened NMR quadrupole-structure lines under DNP at the centers of strain-broadened ESR fine-structure lines, where the ESR and NMR strain broadenings are mutually correlated. Important features of our theoretical model consist of employing the standard Solid Effect associated with an inhomogeneously broadened ESR line, adopting a shell of influence for the electron and nuclear coupling during DNP processes, and introducing an ESR and NMR strain correlation parameter. The correlation parameter characterizes the magnitude and direction (sign) of the correlation between the ESR and NMR strain broadenings and gives the relative contributions to the whole-sample NMR strain broadenings due to coherent, long-range NMR strain effects and from random, short-range NMR strain effects.

On the basis of the model, we have obtained analytical expressions for the shapes and intensities of the NMR quadrupole component lines under DNP. These expressions show that (i) the absorption line shape of a given NMR quadrupole component line under DNP is essentially proportional to either the positive or negative of the first-derivative of its thermal-equilibrium signal, depending on the sign of the correlation parameter, (ii) the strain broadening in the NMR lines under DNP can be reduced from that of the thermal-equilibrium signals, and (iii) the intensities of the NMR signals under DNP depend on the magnitude of the correlation parameter.

It has been found that the theoretical results are in good agreement with experimental data on the ^{27}Al NMR quadrupole structures in several ruby ($Al_2O_3:Cr^{3+}$) crystals. The sign of the correlation parameter in all crystals is found to be positive; this means that the ESR fine-structure constant of a Cr^{3+} ion and the average NMR quadrupole coupling constant of the ^{27}Al nuclear spins contained within the shell of influence of the Cr^{3+} ion are simultaneously deviated to values which are greater or less in magnitude than the perfect-crystal coupling constants. The magnitudes of the correlation parameter are found to be in the vicinity of 0.6, indicating that contributions to the whole-sample strain broadening in the ^{27}Al NMR lines due to the random, short-range strain effects and due to the coherent, long-range strain effects are roughly the same.

As a result of this and our earlier related work, it can be concluded that the DNP method is firmly established both quantitatively and qualitatively for the study of the correlated strain effect between dilute paramagnetic ions and concentrated nuclear spins in single crystalline solids.

---

*Research supported by the National Science Foundation.

†Based on work performed by C. M. Brodbeck in partial fulfillment of the requirements for the degree of Doctor of Philosophy in Physics at Saint Louis University.

‡Present address: University of Marburg, Germany.

[1]A. M. Stoneham, Rev. Mod. Phys. 41, 82 (1969).
[2]J. W. Orton, P. Auzins, J. H. E. Griffiths, and J. E. Wertz, Proc. Phys. Soc. Lond. 78, 554 (1961).
[3]D. H. McMahon, Phys. Rev. 134, A128 (1964).
[4]E. R. Feher, Phys. Rev. 136, A145 (1964).
[5]R. F. Wenzel and Y. W. Kim, Phys. Rev. 140, A1592 (1965).
[6]C. J. Kirkby and J. S. Thorp, J. Phys. C 1, 913 (1968).
[7]S. R. P. Smith, F. Dravnieks, and J. E. Wertz, Phys. Rev. 178, 471 (1969).
[8]R. G. Shulman, B. J. Wyluda, and P. W. Anderson, Phys. Rev. 107, 953 (1957).
[9]E. A. Faulkner and R. K. Ham, Philos. Mag. 7, 279 (1962).
[10]L. E. Drain, Proc. Phys. Soc. Lond. 88, 111 (1966).
[11]B. R. McCart and R. G. Barnes, J. Chem. Phys. 48, 127 (1968).
[12]B. A. Greenberg, Phys. Status Solidi 17, 673 (1966).
[13]A. M. Stoneham, Proc. Phys. Soc. Lond. 89, 909 (1966).

[14]A. M. Stoneham, in *Proceedings XIV Colloque Ampère, Ljubljana*, edited by R. Blinc (North-Holland, Amsterdam, 1967).
[15]Y. Fukai, J. Phys. Soc. Jap. 18, 1413 (1963).
[16]M. F. Lewis and A. M. Stoneham, Phys. Rev. 164, 271 (1967).
[17]R. W. Astrue and H. O. Hooper, Phys. Rev. 164, 1206 (1967).
[18]O. Kanert, Phys. Status Solidi 30, 127 (1968).
[19]O. Kanert, D. Kotzur, and M. Mehring, Phys. Status Solidi 36, 291 (1969).
[20]N. Laurance, E. C. McIrvine, and J. Lambe, J. Phys. Chem. Solids 23, 515 (1962).
[21]P. F. Liao and S. R. Hartmann, Phys. Rev. B 8, 69 (1973).
[22]P. R. Locher and S. Geschwind, Phys. Rev. Lett. 11, 333 (1963).
[23]A. H. Cottrell, *Theory of Crystal Dislocations* (Gordon and Breach, New York, 1964).
[24]C. M. Brodbeck, H. H. Niebuhr, and Sook Lee, Phys. Rev. B 5, 19 (1972).
[25]See, for example, A. Abragam and B. Bleaney, *Electron Paramagnetic Resonance of Transition Ions* (Oxford U. P., London, 1970).
[26]See, for example, M. H. Cohen and F. Reif, in *Solid State Physics*, edited by F. Seitz and D. Turnbull (Academic, New York, 1957), Vol. 5.
[27]E. F. Taylor and N. Bloembergen, Phys. Rev. 113, 431 (1959).
[28]W. I. Dobrov, Phys. Rev. 134, A734 (1964).
[29]R. B. Hemphill, P. L. Donoho, and E. D. McDonald, Phys. Rev. 146, 329 (1966).
[30]The term "shell of influence" as originally used by T. J. Schmugge and C. D. Jeffries, Phys. Rev. 138, A1785 (1965), has a somewhat different meaning from that employed here.
[31]See, for example, C. D. Jeffries, *Dynamic Nuclear Orientation* (Interscience, New York, 1963); A. Abragam and M. Borghini, in *Progress in Low-Temperature Physics*, edited by C. J. Gorter (North-Holland, Amsterdam, 1964), Vol. 4.
[32]Based on standard methods of evaluating rigid-lattice dipolar line broadenings [J. H. Van Vleck, Phys. Rev. 74, 1168 (1948); K. Kambe and J. F. Ollum, J. Phys. Soc. Jap. 11, 50 (1956)], we have calculated that the rigid-lattice nuclear dipolar interactions give rise to second moments for the five NMR quadrupole component lines in the ratio 217 : 289 : 321 : 289 : 217 for $I=\frac{5}{2}$.
[33]A. H. Silver, T. Kushida, and J. Lambe, Phys. Rev. 125, 1147 (1962).
[34]E. O. Schulz-DuBois, Bell System Tech. J. 38, 271 (1959).
[35]W. J. C. Grant and M. W. P. Strandberg, Phys. Rev. 135, A727 (1964).
[36]A. A. Manenkov and V. B. Federov, Zh. Eksp. Teor. Fiz. 38, 1042 (1960) [Sov. Phys.-JETP 11, 751 (1960)].
[37]R. F. Wenzel, Phys. Rev. B 1, 3109 (1970).
[38]H. H. Niebuhr, E. E. Hundt, and E. Brun, Phys. Rev. Lett. 21, 1735 (1968); 22, 159(E) (1969).
[39]H. H. Niebuhr, E. E. Hundt, and E. Brun, Helv. Phys. Acta 43, 777 (1970).
[40]Sook Lee, Phys. Lett. A 26, 572 (1968).
[41]Sook Lee, R. K. Jeck, and V. P. Jacobsmeyer, Phys. Rev. Lett. 21, 515 (1968).
[42]The unusual line shapes observed for the ^{27}Al NMR quadrupole structure in Ref. 41, which was attributed to the Δ^2/δ effect, arose in large part from the magnetic-field-inhomogeneity effect. If there were any contribution from the Δ^2/δ effect, it would have been very small.
[43]C. M. Brodbeck and Sook Lee, Bull. Am. Phys. Soc. II 19, 486 (1974).